Crystal-field energy level analysis for Nd^{3+} ions at the low symmetry C_1 site in $[Nd(hfa)_4(H_2O)](N(C_2H_5)_4)$ single crystals

2008 J. Phys.: Condens. Matter 20 385205

(http://iopscience.iop.org/0953-8984/20/38/385205)

J. Phys.: Condens. Matter **20** (2008) 385205 (13pp) doi:10.1088/0953-8984/20/38/385205

Crystal-field energy level analysis for Nd^{3+} ions at the low symmetry C_1 site in $[Nd(hfa)_4(H_2O)](N(C_2H_5)_4)$ single crystals

Agnieszka Mech[1], Zbigniew Gajek[1], Mirosław Karbowiak[2,4] and Czesław Rudowicz[3]

[1] Institute of Low Temperature and Structure Research, Polish Academy Of Sciences, ulica Okólna 2, 54-422 Wrocław, Poland
[2] Faculty of Chemistry, University of Wrocław, ulica F Joliot-Curie 14, 50-383 Wrocław, Poland
[3] Institute of Physics, Szczecin University of Technology, Aleja Piastów 17, 70–310 Szczecin, Poland

E-mail: karb@wchuwr.pl

Received 11 June 2008, in final form 4 August 2008
Published 21 August 2008
Online at stacks.iop.org/JPhysCM/20/385205

Abstract

Optical absorption measurements of Nd^{3+} ions in single crystals of $[Nd(hfa)_4(H_2O)](N(C_2H_5)_4)$ (hfa = hexafluoroacetyloacetonate), denoted Nd(hfa) for short, have been carried out at 4.2 and 298 K. This compound crystallizes in the monoclinic system (space group $P2_1/n$). Each Nd ion is coordinated to eight oxygen atoms that originate from the hexafluoroacetylacetonate ligands and one oxygen atom from the water molecule. A total of 85 experimental crystal-field (CF) energy levels arising from the Nd^{3+} ($4f^3$) electronic configuration were identified in the optical spectra and assigned. A three-step CF analysis was carried out in terms of a parametric Hamiltonian for the actual C_1 symmetry at the Nd^{3+} ion sites. In the first step, a total of 27 CF parameters (CFPs) in the Wybourne notation B_{kq}, admissible by group theory, were determined in a preliminary fitting constrained by the angular overlap model predictions. The resulting CFP set was reduced to 24 specific independent CFPs using appropriate standardization transformations. Optimizations of the second-rank CFPs and extended scanning of the parameter space were employed in the second step to improve reliability of the CFP sets, which is rather a difficult task in the case of no site symmetry. Finally, seven free-ion parameters and 24 CFPs were freely varied, yielding an rms deviation between the calculated energy levels and the 85 observed ones of 11.1 cm^{-1}. Our approach also allows prediction of the energy levels of Nd^{3+} ions that are hidden in the spectral range overlapping with strong ligand absorption, which is essential for understanding the inter-ionic energy transfer. The orientation of the axis system associated with the fitted CF parameters w.r.t. the crystallographic axes is established. The procedure adopted in our calculations may be considered as a general framework for analysis of CF levels of lanthanide ions at low (triclinic) symmetry sites.

1. Introduction

The lanthanide(III) β-diketonates make up an important group of compounds due to their potential applications as luminescent and laser materials, efficient organic light emitting diodes (OLEDs) [1], and polymer light emitting diodes (PLEDs) [2]. These compounds are known to possess a high internal quantum efficiency, which is evidenced by the observation of the laser action of europium benzoylacetonate

[4] Author to whom any correspondence should be addressed.

in solution [3]. In this type of material the organic ligand is an absorbing component, whereas the lanthanide ion is an emitting one. Therefore, their quantum yield depends on efficiency of the energy transfer processes between organic ligands and the lanthanide ion. These intramolecular energy transfer processes can be modeled theoretically to estimate the quantum efficiency [4]. Such modeling is indispensable for development of new, efficient light converting molecular devices (LCMDs). The main energy transfer channels are those in which the $4f^N$ lanthanide ion levels, positioned at energy similar to that of the lowest triplet and singlet ligand states, participate. However, these lanthanide levels usually cannot be observed experimentally, since they are obscured by strong and broad ligand absorption bands. Therefore, the ability to predict by model calculations the positions of the levels participating in the energy transfer, using other available experimental data, is crucial. For this purpose crystal-field (CF) analysis based on a parametric Hamiltonian proved to be a very successful tool [5, 6].

In this paper a semiempirical parametric Hamiltonian, including free-ion and CF terms, is used for interpretation and calculation of energy levels of the $4f^3$ configuration of Nd^{3+} in $[Nd(hfa)_4(H_2O)](N(C_2H_5)_4)$, denoted Nd(hfa) for short. This compound crystallizes in the monoclinic system (space group $P2_1/n$). Each neodymium ion is nine coordinated by oxygen atoms—eight of them originating from the four hexafluoroacetylacetonate chelating ligands and one from the water molecule. The local symmetry at the Nd^{3+} ion site may be described as triclinic C_1 symmetry, so in fact there is no symmetry element except identity.

For such low symmetry systems it is very difficult to perform CF analysis and parameter fits, so analysis of the energy levels of lanthanide ions at triclinic (C_1, C_i) and even monoclinic (C_s, C_2, C_{2h}) symmetry sites has been hitherto attempted only in a few cases (for references see, e.g., [7]). The present paper addresses the most important difficulties arising in CF analysis, which bear on the reliability of CFPs. Firstly, fittings may return numerous local minima, whereas the final solutions usually depend strongly on the starting parameter values. In view of the existence of numerous local minima, a question arises of how to differentiate between the global minimum and the spurious ones. To obtain reliable starting CFPs, the angular overlap model (AOM) [8–10] was applied in the initial phase of CF analysis. This model is especially useful for low symmetry systems, since in this step the CF effects may be described by means of three (or fewer) effective parameters only, being linear combinations of 27 B_{kq} parameters. Further, for systems with no symmetry elements, there exist an infinite number of choices of the orientation of the axis system. Each choice corresponds to a specific CFP set distinct for a given axis system. Therefore, it is desirable to specify the axis system used in each phase of the calculations, to avoid misleading ambiguities. We combine several approaches [11–13] pertinent to low symmetry CF calculations. In particular, we apply Burdick and Reid's procedure [11] to reduce the number of CFPs from 27 CFPs admissible by group theory for triclinic symmetry to 24 specific independent CFPs and employ the multiple correlated fitting technique (MCFT) [14, 7, 15]. This method has been shown to lower the risk of being misled by false minima, at almost no additional computational cost in comparison with the conventional methods. The concept of standardization of CF Hamiltonians [12, 14], based on limiting the ratio $\mathrm{Re}\, B_{22}/B_{20}$ (in Wybourne notation) to the standard range, i.e. equivalently to the maximal values of B_{k0} axial parameters [13], is utilized for determination of the orientation of the coordinate frame in which the final CFPs are expressed [7].

The paper is organized as follows. In section 2 the experimental aspects are presented, whereas the theoretical background and nomenclature are briefly outlined in section 3. Experimental absorption spectra are presented and analyzed in section 4. Discussion of the results, including the energy levels and CF strength and the Hamiltonian parameters, as well as the nominal axis system and the crystallographic one, is provided in section 5. Finally, a summary and conclusions are provided in section 6.

2. Experimental aspects

The starting materials were $NdCl_3{\cdot}6H_2O$ (99.99%, Aldrich), 1,1,1,5,5,5-hexafluoro-2,4-pentanedione (hexafluoroacetylacetone) (99%, Aldrich) and $N(C_2H_5)_4Cl$ monohydrate (99.8%, Merck). The compound $[Nd(hfa)_4(H_2O)](N(C_2H_5)_4)$ was prepared by deprotonating 22 mmol of the hexafluoroacetylacetone ligand with NaOH in absolute ethanol, followed by addition of 10 mmol of ethanolic solution of $N(C_2H_5)_4Cl$, and subsequent dropwise addition of 5 mmol of the $NdCl_3{\cdot}6H_2O$ also dissolved in absolute ethanol. The sodium chloride, which precipitates immediately after the first drop of the counter-ion is added to the solution, was filtered off. The thus-obtained solution was concentrated by heating until the crystallization started. Afterward, a small amount of absolute ethanol was added to dissolve the solid and this clear solution was then left at room temperature overnight. The light-violet single crystals of a good optical quality formed in this way were separated by filtering and then dried in air at room temperature.

Electronic absorption spectra were recorded on a Cary 50 UV–vis–NIR spectrophotometer in the 2500–28 000 cm^{-1} range. For the low temperature measurements the crystal was mounted in a helium Oxford Instruments optical cryostat and cooled to ∼4.2 K. Unpolarized absorption spectra were measured for random orientation of the crystal at 4.2 and 298 K.

3. Theoretical background and nomenclature

For the energy level calculations and fitting the observed energy levels we apply the effective operator approach [16, 17], suitable for $4f^N$ ions in crystals and based on diagonalization of the total Hamiltonian $\hat{H} = \hat{H}_{\mathrm{FI}} + \hat{H}_{\mathrm{CF}}$, i.e. the

free-ion ($\hat{H}_{\rm FI}$) and crystal-field ($\hat{H}_{\rm CF}$) Hamiltonian. $\hat{H}_{\rm FI}$ is given by [6, 16, 17]

$$\hat{H}_{\rm FI} = E_{\rm ave} + \sum_{k=2,4,6} F^k(nf,nf)\,\hat{f}_k + \zeta_{4\rm f}\hat{A}_{\rm SO} + \alpha\hat{L}(\hat{L}+1) + \beta\hat{G}(G_2) + \gamma\hat{G}(R_7) + \sum_{i=2,3,4,6,7,8} T^i\hat{t}_i + \sum_{j=0,2,4} M^j\hat{m}_j + \sum_{k=2,4,6} P^k\hat{p}_k \quad (1)$$

where $E_{\rm avg}$ is the spherically symmetric one-electron part and $F^k(nf,nf)$ and $\zeta_{4\rm f}$ are the radial parts of the electrostatic and spin–orbit interactions, whereas $\hat{f}_k$ and $\hat{A}_{\rm SO}$ are the angular parts of these interactions, respectively. The α, β, and γ parameters (not to be confused with the Euler angles (α, β, and γ) used later) account for the radial interactions not transforming as $\hat{f}_k$ and are associated with the two-body correction terms. $\hat{G}(G_2)$ and $\hat{G}(R_7)$ denote Casimir operators for the groups G_2 and R_7, respectively, whereas L is the total orbital angular momentum. The three-particle configuration interaction is expressed by $T^i\hat{t}_i$ ($i = 2, 3, 4, 6, 7, 8$), where T^i are parameters and $\hat{t}_i$ are three-particle operators. The operators $\hat{p}_k$ (and parameters P^k) represent the electrostatically correlated spin–orbit perturbation, whereas $\hat{m}_j(M^j)$ the spin–spin and spin–other-orbit relativistic corrections [16, 17].

The crystal-field Hamiltonian $\hat{H}_{\rm CF}$ can be expressed as [6, 16, 17]

$$\hat{H}_{\rm CF} = \sum_{k,q} B_{kq}\hat{C}^{(k)}_q \quad (2)$$

where $\hat{C}^{(k)}_q$ are the normalized spherical-tensor operators of rank k and component q, B_{kq} are the crystal-field parameters (CFPs), and $k = 2$, 4, and 6. For C_1 site symmetry $-6 \leqslant q \leqslant +6$. For a review of the operator and parameter notations used in the EMR and optical spectroscopy area, see [18]. The $\pm q$ parameters are related by $B_{k-q} = (-1)^q B^*_{kq}$ and B_{kq} is commonly presented as $B_{kq} = \mathrm{Re}\,B_{kq} + \mathrm{i}\,\mathrm{Im}\,B_{kq}$; see, e.g., [19]. The crystal-field levels are obtained by simultaneous diagonalization of the matrix of the Hamiltonian in (1) and (2) within the basis functions $|\mathrm{SLJ}M_J\rangle$, which for the $4f^3$ configuration has the dimension of 364. The f-shell computer package developed by Reid [20] was used in our calculations.

The Nd ion site in the compound under study has no symmetry elements, thus according to group theory all 27 parameters B_{kq} ($k = 2, 4, 6$; $q = -k, \ldots, k$) appear in equation (2). Since no specific symmetry adopted axis system [7] exists in this case, any rotation of the axis system by three Euler angles (α, β, γ) yields physically equivalent sets of CFPs [7, 11]. Therefore, the number of independent CFPs may be reduced by three as Burdick and Reid noticed [11], inspired by the discussion by Linehan and Stedman [21] of symmetries of irreducible representations. The method [11] and the 3DD method proposed in [22] (see also [23]) may be used to perform this reduction. We employ the first method for the full set of 27 CFPs determined from the AOM calculations and the subsequent fittings.

The authors [11] suggested first elimination of B_{21}, i.e. both the real and imaginary parts, by a rotation α/Oz about the initial z axis of the system and a rotation β/Ox' about the x axis, and next of Im B_{22} by a rotation γ/Oz'' about the new z axis. Note that definition of Euler angles used in [22, 23] differs from that in [11] also used here.

The two Euler angles α and β are determined from the set of equations

$$\mathrm{Re}\,B'_{21} = -\frac{\sqrt{6}}{4}\sin 2\beta\, B_{20} + \cos 2\beta\,(\cos\alpha\,\mathrm{Re}\,B_{21} + \sin\alpha\,\mathrm{Im}\,B_{21}) + \tfrac{1}{2}\sin 2\beta\,(\cos 2\alpha\,\mathrm{Re}\,B_{22} + \sin 2\alpha\,\mathrm{Im}\,B_{22}) = 0 \quad (3)$$

$$\mathrm{Im}\,B'_{21} = \cos\beta\,(-\sin\alpha\,\mathrm{Re}\,B_{21} + \cos\alpha\,\mathrm{Im}\,B_{21}) + \sin\beta\,(-\sin 2\alpha\,\mathrm{Re}\,B_{22} + \cos 2\alpha\,\mathrm{Im}\,B_{22}) = 0, \quad (4)$$

where Re B'_{21} and Im B'_{21} are obtained by rotation by only the two Euler angles α and β determined from equations (3) and (4). In general, the transformations of CFPs B^k_q follow from the transformation properties of the operators in equation (2) and are given by the Wigner rotation matrices $D^{(k)}_{qq'}(\alpha,\beta,\gamma)$, being the irreducible representations of the full rotation group [13, 24]:

$$B'_{kq} = \sum D^{(k)}_{qq'}(\alpha,\beta,\gamma)\,B_{kq}. \quad (5)$$

In particular, for the angles α, β, determined from (3) and (4) ($\gamma = 0$),

$$\mathrm{Re}\,B'_{22} = \left(\cos(2\alpha)(\cos^2(2\beta)+1)/2\right)\mathrm{Re}\,B_{22} - (\sin(2\beta)\cos(\alpha)/8)\,\mathrm{Re}\,B_{21} + (3/2)^{1/2}(3\cos^2(\beta)-1)B_{20} + (\sin(2\beta)\sin(\alpha)/8)\,\mathrm{Im}\,B_{21} + \sin(2\alpha)\sin(2\beta)\,\mathrm{Im}\,B_{22} \quad (6)$$

$$\mathrm{Im}\,B'_{22} = -\sin(2\alpha)\cos(\beta)\,\mathrm{Re}\,B_{22} + (\sin(\beta)\sin(\alpha)/4)\,\mathrm{Re}\,B_{21} - (\sin(\beta)\cos(\alpha)/4)\,\mathrm{Im}\,B_{21} + \cos(2\alpha)\cos(\beta)\,\mathrm{Im}\,B_{22}. \quad (7)$$

The γ angle required to set the parameter Im B'_{22} to zero is determined from the ratio [6, 11]

$$\tan(2\gamma) = \mathrm{Im}\,B'_{22}/\,\mathrm{Re}\,B'_{22}. \quad (8)$$

The equations (3) and (4) have been shown to provide three solutions corresponding to a minimum, a maximum and a saddle point of the B'_{20} (α,β) function [11]. Equation (8), in turn, yields two values for γ that differ from each other by 90°. Thus, there are six possible solutions of (3) and (4), which can be transformed into each other by appropriate standardization transformations $S2$–$S6$ defined in [12] and [14]. Thus these solutions correspond directly to the six orientations of the axis system, $S1$–$S6$ defined earlier in [11]; see also [7] and [14]. Hence the method based on finding zeros of the derivatives of the parameters B_{k0} leads to several physically equivalent but numerically distinct parameter sets.

In order to determine the starting values of B_{kq} parameters, the angular overlap model (AOM) has been applied [25]. In this model the CF parameters B_{kq}, equation (2), are expressed in terms of the factors $W^{\tau\mu}_{kq}$, which

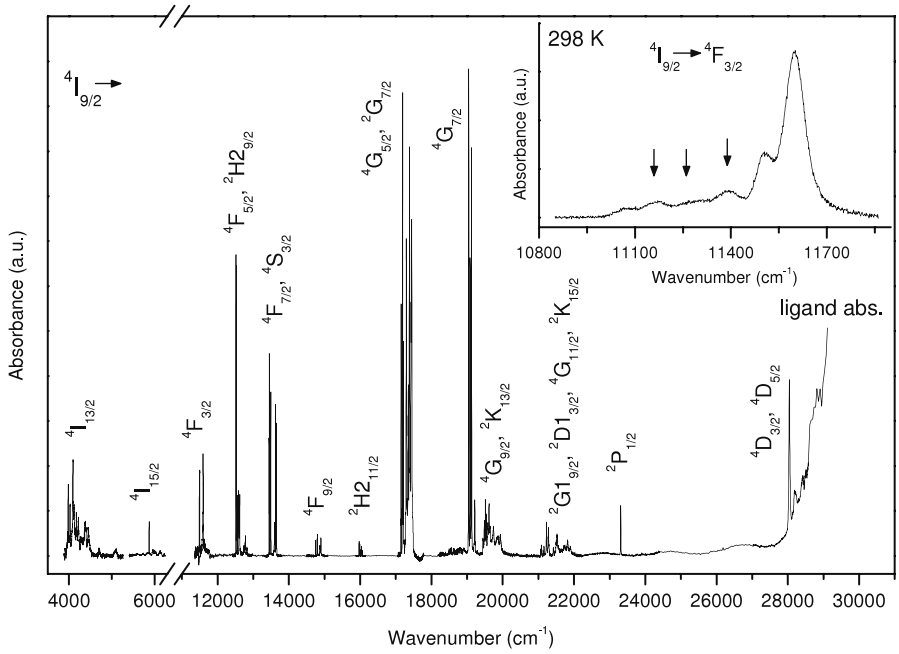

Figure 1. Electronic absorption spectrum recorded at 4.2 K for a $[Nd(hfa)_4(H_2O)](N(C_2H_5)_4)$ single crystal. All transitions start from the ground state $^4I_{9/2}$ of Nd^{3+} and the terminal multiplets are labeled as indicated. The inset shows the spectrum measured at room temperature in the $^4I_{9/2} \rightarrow {}^4F_{3/2}$ transition range; arrows indicate the hot bands displaced by 204, 355, and 426 cm^{-1} from the 11 600 cm^{-1} line.

depend on the geometry of the metal ion surroundings, and the AOM parameters e^{τ}_{μ}, which account for contributions due to particular ligands [10]:

$$B_{kq} = \sum_{\mu,\tau} W^{\tau\mu}_{kq} e^{\tau}_{\mu} \tag{9}$$

where $\mu = 0, 1, 2$; in our case, τ = O(ketone) or O(H_2O), whereas

$$W^{\tau\mu}_{kq} = [(2k+1)/7] \begin{pmatrix} 3 & k & 3 \\ 0 & 0 & 0 \end{pmatrix}^{-1} (-1)^{\mu}(2-\delta_{\mu 0}) \times \begin{pmatrix} 3 & k & 3 \\ -\mu & 0 & \mu \end{pmatrix} \sum_{t_\tau} C^k_q\left(\Theta_{t_\tau}, \Phi_{t_\tau}\right) s^{t_\tau}_{\mu}. \tag{10}$$

The index τ identifies ligands and t_τ distinguishes different positions of the type τ ligands in the coordination polyhedron; μ represents the absolute value of the magnetic quantum number of a 4f electron in the local axis system—μ takes the values 0, 1 and 2, denoted also by σ, π and δ, respectively. The $s^{t\tau}_{\mu}$ are the ratios of the AOM parameters determined from the first principle calculations [10] and account for various ML_τ distances in the first coordination sphere. Thus, if one does not differentiate between O(ketone) and O(H_2O), there are three AOM parameters e^{τ}_{μ} (τ = O, $\mu = \sigma$, π and δ) required to describe the Nd–O interaction in the local metal–ligand axis system.

To facilitate the comparison of CFP sets obtained from different calculation steps, we use the CFP strength, s_k ($k = 2, 4, 6$) and s_{cf}, defined as [26]

$$s_k = \left[(2k+1)^{-1}\left((B_{k0})^2 + 2\sum_{q>0}\left((\mathrm{Re}\, B_{kq})^2 + (\mathrm{Im}\, B_{kq})^2\right)\right)\right]^{1/2},$$
$$s_{cf} = \left[(1/3)\sum_k s_k^2\right]^{1/2}. \tag{11}$$

These quantities represent the rotational invariants of the second-rank CFPs [7].

4. Results

4.1. Absorption spectra

Figure 1 presents a sample absorption spectrum recorded at 4.2 K in the 3500–30 000 cm^{-1} range. The observed Nd^{3+} ion lines result from the intraconfigurational $4f^3 \rightarrow 4f^3$ transitions from the lowest Stark component of the ground $^4I_{9/2}$ multiplet to the crystal-field levels of the excited $^{2S+1}L_J$ multiplets. The SLJ labels of the terminal levels are indicated in figure 1.

The high-resolution absorption spectra at 4.2 K shown in figures 2(a)–(c) correspond to the $^4I_{9/2} \rightarrow {}^4F_{3/2}$, $^4I_{9/2} \rightarrow {}^4F_{9/2}$ and $^4I_{9/2} \rightarrow {}^2H2_{11/2}$ transitions, respectively. The number of observed lines is equal to 2, 5 and 6, respectively, as expected from the crystal-field theory predictions for the splitting of the terminal $^{2S+1}L_J$ multiplet into $(2J+1)/2$ components (Kramers' doublets) for a Nd^{3+} ion at the C_1 symmetry site. Similarly, also in other spectral regions the number of observed transitions to the given $^{2S+1}L_J$ multiplet does not exceed $(2J+1)/2$. This observation, together with the appearance of the $^4I_{9/2} \rightarrow {}^2P_{1/2}$ transition as a single sharp peak at

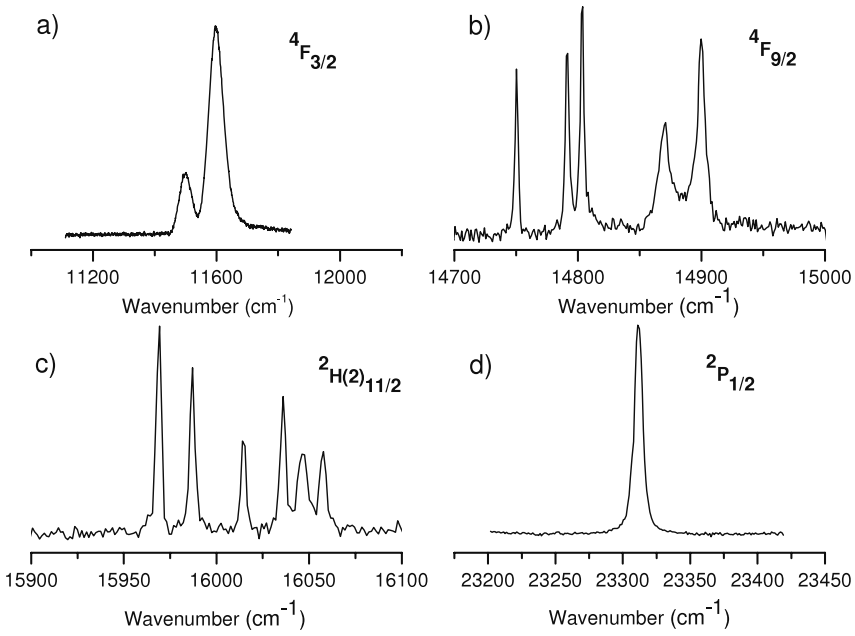

Figure 2. Absorption spectra at 4.2 K showing the transitions from the ground state $^4I_{9/2}$ to the excited multiplets of Nd^{3+} in $[Nd(hfa)_4(H_2O)](N(C_2H_5)_4)$: (a) $^4F_{3/2}$, (b) $^4F_{9/2}$, (c) $^2H2_{11/2}$, and (d) $^2P_{1/2}$.

23 312 cm^{-1} with an FWHM of 6 cm^{-1} (see figure 2(d)), is indicative of a single neodymium site, in accordance with the crystal structure data. The low symmetry of the Nd^{3+} ion environment results in the absence of vibronic lines in the electronic absorption spectrum.

Since there is one water molecule in the first Nd^{3+} coordination sphere, the emission from the excited states is very efficiently quenched by the multiphonon relaxation processes with participation of OH vibrations. Thus the splitting of the $^4I_{9/2}$ ground multiplet could not be determined from luminescence measurements. However, from analysis of the hot bands in the absorption spectrum observed at 298 K in the region of the $^4I_{9/2} \rightarrow {}^4F_{3/2}$ (inset in figure 1) and $^4I_{9/2} \rightarrow {}^2P_{1/2}$ transitions, the three CF components of the $^4I_{9/2}$ ground multiplet have been assigned at 204, 355 and 426 cm^{-1}. Thus, examination of the absorption spectrum enables determination of a total of 85 experimental energy levels of Nd^{3+} in Nd(hfa), which form a data set used in CF calculations presented in section 4.2.

4.2. Energy level calculations

The geometrical coefficients $W_{kq}^{\tau\mu}$ in equation (10) were calculated using the crystallographic data reported for $[Nd(hfa)_4(H_2O)](N(C_2H_5)_4)$ in [27]. The Cartesian coordinates of ligating atoms forming the first coordination sphere in the axis system adopted in our calculations are listed in table 1. The z axis is chosen along the crystallographic b axis (figure 3(a)).

Having determined the coefficients $W_{kq}^{\tau\mu}$, the 27 B_q^k parameters were expressed using equation (9) in terms of three AOM parameters e_μ^{O} ($\mu = \sigma$, π and δ). Then, in the first step of our analysis, values of the AOM parameters e_μ^{O} were fitted to the experimental energy levels as $e_\sigma^{\mathrm{O}} = 1052(32)$, $e_\pi^{\mathrm{O}} = 656(31)$, and $e_\delta^{\mathrm{O}} = 292(29)$ (in cm^{-1}). Since, for Nd^{3+} ions at C_1 symmetry sites, the Kramers doublets are not distinguishable, they were assigned by relating the calculated energies to the experimental ones, multiplet after multiplet with increasing energies. In the case when the number of levels was smaller than that predicted by theory, the experimental levels were assigned to the nearest calculated values. These AOM parameters yield CFPs B_{kq}, which could serve as the initial ones in the next calculation step. However, we realized, that prior to this it is advisable to introduce an additional 'optimization' step. For this, the contributions from the second-rank parameters were excluded from AOM parameters and we vary freely the CFPs B_{2q} ($q = 0, 1, 2$) together with the modified $e_\sigma^{\mathrm{O}\prime}$, $e_\pi^{\mathrm{O}\prime}$ and $e_\delta^{\mathrm{O}\prime}$ AOM parameters. We have searched for the best minima changing the starting values of B_{2q} ($q = 0$, 1, 2) from -500 to 500 cm^{-1} in different combinations, with a step of 50 cm^{-1}. In this way we localized six minima with the lowest rms deviations between 11.0 and 11.3 cm^{-1}, which were characterized by very similar values of $e_\sigma^{\mathrm{O}\prime}$, $e_\pi^{\mathrm{O}\prime}$ and $e_\delta^{\mathrm{O}\prime}$

Table 1. Cartesian coordinates of the bonding β-diketone's oxygens (O1–O8) and the water molecule oxygen (O9), in the axis system centered at the Nd^{3+} ion, used for calculations of the AOM $W_{kq}^{\tau\mu}$ coefficients in equation (8).

Ligand	x	y	z
O1	1.4755	−1.7709	−0.8399
O2	0.4710	−1.5931	1.7834
O3	−0.2962	2.4483	−0.1220
O4	0.8776	0.8814	−2.1698
O5	2.3017	0.7557	0.2759
O6	0.3116	1.0761	2.2116
O7	−1.2945	−2.1144	−0.5162
O8	−2.1231	−0.1090	1.2595
O9	−1.9088	0.4874	−1.6509

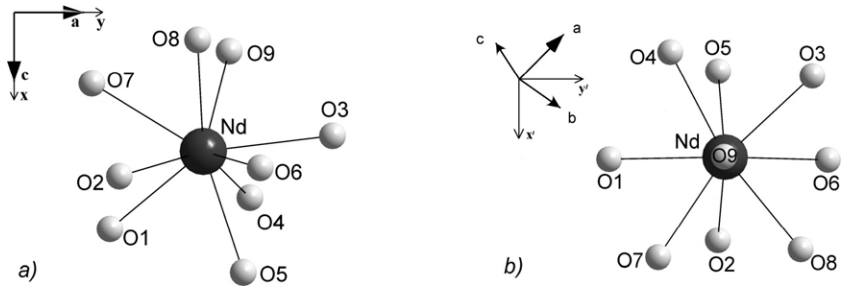

Figure 3. (a) The axis system used in our calculations of the geometrical coefficients in equation (9). The z axis is chosen along the crystallographic b axis; (b) the axis system rotated in a such way that the new z' axis passes through the O(9) oxygen atom.

(and thus also fourth- and sixth-rank B_{kq} parameters) but differ considerably in values of the second-rank CFPs.

For each of these six solutions we calculated B_{kq} ($k = 4,\ 6$) parameters. The optimized second-rank CFPs were then used to calculate the Euler angles of the rotations required to eliminate the CFPs Re B_{21}, Im B_{21} and Im B_{22} using equations (3), (4) and (8). The 24 thus-obtained B_{kq} parameter sets were subsequently fitted to 85 experimental energy levels. Two solutions with the lowest rms deviation of 11.1 cm^{-1} yielded the same CFP values, but differed only by Euler angles required to eliminate three second-rank CFPs. As the best solution we have chosen the one closest to the starting parameter values. For quantitative comparison of CFP sets we calculated the closeness factors C_k ($k = 2, 4, 6$) and the global factor C_{gl} defined in [7]. The starting CFPs resulting from this 'optimization' step and yielding the best solution are listed in table 2, column AOM–B_{kq}.

Equations (3), (4), and (8) yield six possible solutions for the Euler angles of the rotations required to eliminate the CFPs Re B_{21}, Im B_{21}, and Im B_{22}. For the AOM–B_{kq} CFP set we chose the angles $\alpha = -36.72°$, $\beta = -77.37°$, and $\gamma = -49.12°$, corresponding to the maximum value of B'_{20}.

The AOM–B_{kq} CFPs transformed by the rotations (α, β, γ) using equation (5) are given in table 2 column $S1$. Five remaining equivalent sets $S2$–$S6$, corresponding to other possible orientations of the coordinate system, were generated using the package CST [28] and are also listed in table 2. The sets can be transformed into each other by appropriate rotations $S2$–$S6$ defined in [12] and [14]. They correspond to the maximum B_{20} value ($S1$ and $S3$), the minimum value of B_{20} ($S4$ and $S6$), and the saddle point value ($S2$ and $S5$).

All sets $S1$–$S6$ in table 2 represent numerically distinct yet implicitly physically equivalent solutions. Each correlated set belongs to a different region of the multiparameter space and yields the same energy levels. These sets and additionally several slightly modified counterpart sets (not listed) were used as the initial sets for a number of additional independent fittings in different regions of the multiparameter space.

Thus, 24 C_1 symmetry CFPs (of each set), together with the free-ion parameters E_{avg}, F^k ($k = 2,\ 4,\ 6$), $\zeta_{4\mathrm{f}}$, α, and β, were simultaneously fitted to the 85 experimentally observed Stark components. In general, this procedure yields one standard CFP set ($S4$ in our case) and five non-standard CFP sets, each set being independently fitted. Here, the term '*standard*' refers to any CFP set for which, according to the standardization idea [12, 14], the ratio Re B_{22}/B_{20} (in Wybourne notation) is confined to the range $(0,\ 1/\sqrt{6})$. The fitted non-standard sets, here $S1$, $S2$, $S3$, $S5$, and $S6$, were back-transformed using the package CST [28] into the standard region. It turned out that all transformed sets were very close, to within a few cm^{-1}, to the standard set $S4$. The six independently fitted and standardized CFPs were averaged and the resulting set is listed in table 2 column Fit-avg. The errors in determination of the parameter values given in the parentheses in table 2 are the average values of the six fitting errors for the sets Si ($i = 1$–6). The corresponding energy levels calculated using the Fit-avg set are listed together with the experimental levels in table 3.

Note that in each step of our fitting procedure not only the appropriate CFPs but also the free-ion parameters, E_{avg}, F^2, F^4, F^6, $\zeta_{4\mathrm{f}}$, α, and β, were varied freely. Their final values, averaged over six fittings in the regions $S1$–$S6$, are listed in the caption of table 2.

5. Discussion

5.1. Energy levels and CF strength

The lines observed in the absorption spectrum of Nd(hfa) in the 3500–30 000 cm^{-1} region at 4.2 K are due to the $4f^3 \rightarrow 4f^3$ transitions within the CF levels originating from 25 free-ion multiplets of the Nd^{3+} ion. The analysis of this spectrum enables determination of 85 energy levels listed in table 3, column 3, which were included in the fittings. The edge of the strong ligand absorption bands is observed at energy above 28 000 cm^{-1} (figure 1). These bands obscure the transitions to the $4f^3$ levels located in this region. Lack of precise positions of these levels hinders assessment of energy transfer rates between the ligands and the Ln^{3+} ions and calculations of the emission quantum efficiency for this type of complex [4]. It has been shown [30], however, that even on the basis of a truncated dataset, i.e. composed of the energy levels that are experimentally determinable—usually in the lower energy range of the spectrum, the obtained CFPs can quite well predict the positions of CF levels in the higher energy range of the spectrum, i.e. those which cannot be observed due to the overlap with, for instance, strong f–d, charge transfer, or ligand absorption bands. For Nd(hfa) the largest difference between calculated and experimental energy levels does not exceed 29 cm^{-1} in the analyzed energy region

Table 2. Crystal-field parameters (in cm^{-1}) for Nd^{3+} in $[Nd(hfa)_4(H_2O)](N(C_2H_5)_4)$: starting (AOM–$B_{kq}$), transformed ($Si$, $i = 1$–6), and fitted (using 85 experimental energy levels: Fit-avg). (Note that the rms deviation between the calculated and observed energies is 11.1 cm^{-1}. The s_k values (in cm^{-1}) for AOM–B_{kq} and S_i ($i = 1$–6) sets are $s_2 = 247$, $s_4 = 301$ and $s_6 = 415$, whereas for the fitted Fit-avg set $s_2 = 250$, $s_4 = 309$, $s_6 = 418$. The E_{avg}, F^2, F^4, F^6, ζ_{4f}, α and β free-ion parameters were freely varied in fittings together with the appropriate CFPs, and they assumed the following values (averaged over six fittings in $S1$–$S6$ regions; see the text) (in cm^{-1}): $E_{avg} = 24298(2)$, $F^2 = 72210(19)$, $F^4 = 52389(42)$, $F^6 = 35508(33)$, $\zeta_{4f} = 878.8(0.7)$, $\alpha = 21.6(0.2)$, $\beta = -638(6)$. Other parameters were kept constant as follows (in cm^{-1}) [30]: $\gamma = 1526$, $T^2 = 303$, $T^3 = 41$, $T^4 = 66$, $T^6 = -289$, $T^7 = 317$, $T^8 = 301$, $M^0 = 1.85$, $M^2 = 1.04$, $M^4 = 0.70$, $P^2 = 232 P^4 = 174$, $P^6 = 116$.)

	AOM–B_{kq}[a]	$S1$[b]	$S2$[c]	$S3$[c]	$S4$[c]	$S5$[c]	$S6$[c]	Fit − avg[d,e]
B_{20}	−112	374	166	374	−540	166	−540	−534(17)
Re B_{21}	−95	0	0	0	0	0	0	0
Im B_{21}	276	0	0	0	0	0	0	0
Re B_{22}	128	−288	−373	288	−85	373	85	−119(16)
Im B_{22}	212	0	0	0	0	0	0	0
B_{40}	58	−152	27	−152	8	27	8	−32(63)
Re B_{41}	−46	−234	−198	−524	240	−410	−140	198(51)
Im B_{41}	327	−524	−410	−234	−140	198	−240	−4(58)
Re B_{42}	−56	12	−101	−12	−113	101	113	−193(48)
Im B_{42}	−64	−60	−132	−60	−162	132	162	−143(61)
Re B_{43}	197	−53	139	25	−27	328	194	−150(59)
Im B_{43}	−151	−25	−328	53	−194	139	−27	−192(56)
Re B_{44}	240	71	−79	71	−63	−79	−63	85(63)
Im B_{44}	414	234	−200	−234	−499	−200	−499	−516(32)
B_{60}	−420	−323	364	−323	−346	364	−346	−381(64)
Re B_{61}	47	137	220	−438	110	231	166	86(75)
Im B_{61}	−462	−438	231	137	166	−220	−110	314(55)
Re B_{62}	−500	376	−555	−376	717	555	−717	624(42)
Im B_{62}	476	−110	15	−110	425	−15	−425	235(5)
Re B_{63}	112	237	−74	−271	−248	−56	242	−537(41)
Im B_{63}	343	271	56	−237	−242	−74	−248	245(71)
Re B_{64}	96	131	314	131	125	314	125	284(48)
Im B_{64}	−120	127	−350	−127	239	−350	239	−15(69)
Re B_{65}	−97	−219	−140	−232	9	512	−191	27(59)
Im B_{65}	383	−232	512	−219	−191	140	−9	−125(67)
Re B_{66}	103	−627	362	627	−122	−362	122	−203(53)
Im B_{66}	143	213	13	213	285	−13	−285	162(55)

[a] CFP set obtained in the fitting to experimental data, with B_{2q} parameters freely varied, while keeping B_{4q} and B_{6q} parameters constrained by the ratios imposed by the AOM model (see the text).

[b] CFP set $S1$ obtained from the AOM–B_{kq} set transformed by the Euler angles $\alpha = -36.72°$, $\beta = -77.37°$ and $\gamma = -49.12°$ in order to reduce second-rank CFPs to zero.

[c] CFP sets $S2 - S6$ obtained from the $S1$ set using the appropriate standardization transformations [12, 14].

[d] Average values of the CFPs fitted using the Reid program [20] in the respective regions Si ($i = 1$–6) of CFP space and subsequently back-transformed to the standard region ($S4$), with Si ($i = 1$–6) sets from the previous columns as the starting CFPs, respectively.

[e] Numbers in parenthesis indicate the errors in determination of the parameter values.

up to 28 416 cm^{-1}, whereas a relatively low rms deviation of 11.1 cm^{-1} is achieved. Such accuracy seems to be sufficient for a reliable prediction of the CF levels in the higher energy region and, consequently, the energy transfer rates between lanthanide ion and ligands or other photophysical properties.

In Nd(hfa) the experimental $^{2S+1}L_J$ multiplets are shifted towards higher energies as compared to those observed for Nd^{3+} in $LaCl_3$ crystal (Nd^{3+} ions are surrounded in $LaCl_3$ by nine chloride ions) [31], suggesting that the Nd–O bonds in Nd(hfa) possess less covalent character than Nd–Cl bonds in La(Nd)Cl_3 (the nephelauxetic effect). Moreover, the overall splittings of $^{2S+1}L_J$ multiplets are significantly larger for Nd(hfa) than those for Nd^{3+}:$LaCl_3$, e.g. the experimental values of $^4I_{9/2}$ ground multiplet splitting are 426 and 249 cm^{-1} [32], respectively. The former value obtained by us for Nd(hfa) is close to the 456 cm^{-1} reported for the $Na_3[Nd(oxydiacetate)_3]\cdot 2NaClO_4\cdot 6H_2O$ compound, where the Nd^{3+} ion is coordinated by six carboxylate and three ether oxygen atoms [32]. The relative strengths of CF interactions for ions in different hosts may be compared in terms of total crystal-field strength parameter, s_{cf}, defined in equation (11). For Nd(hfa) we obtain $s_{cf} = 331.4$ cm^{-1}, whereas for Nd^{3+} ions located at ninefold coordinated sites in other hosts, Nd^{3+}:$LaCl_3$, $[Nd(H_2O)_9](CF_3SO_3)_3$, $Na_3[Nd(oxydiacetate)_3]\cdot 2NaClO_4\cdot 6H_2O$, and $NdAlO_3$, the following values were reported (in cm^{-1}): 176 [33], 237 [33], 419 [33], and 470 [33], respectively. Thus, the crystal-field generated by the ketone oxygen ligands appears stronger than that produced by the water molecules in $Nd(H_2O)_9^{3+}$ or the Cl^- ions in Nd^{3+}:$LaCl_3$, but it is weaker as compared with

Table 3. The energy levels for Nd^{3+} in $[Nd(hfa)_4(H_2O)](N(C_2H_5)_4)$ calculated using the CFP set Fit-avg of table 2 and the experimental ones measured at 4.2 K.

$^{2S+1}L_J$ [a]	Calculated energy (cm^{-1})	Experimental energy (cm^{-1})	$E_{calc.} - E_{exp.}$ (cm^{-1})
$^4I_{9/2}$	1	0	−1
	173	—	—
	215	204	−11
	354	355	1
	427	426	−1
$^4I_{11/2}$	2 021	—	—
	2 074	—	—
	2 098	—	—
	2 120	—	—
	2 171	—	—
	2 188	—	—
$^4I_{13/2}$	3 973	3 981	8
	4 014	4 024	10
	4 065	4 071	6
	4 087	4 091	4
	4 128	4 120	−8
	4 168	4 174	5
	4 229	4 222	−7
$^4I_{15/2}$	5 882	5 874	−8
	5 972	5 960	−12
	6 014	6 004	−10
	6 126	6 131	5
	6 220	6 225	5
	6 269	—	—
	6 383	—	—
	6 493	—	—
$^4F_{3/2}$	11 492	11 495	3
	11 576	11 596	20
$^4F_{5/2} + {}^2H2_{9/2}$	12 514	12 522	8
	12 561	12 561	0
	12 583	12 585	2
	12 610	12 600	−10
	12 625	12 618	−7
	12 731	12 741	10
	12 769	12 780	11
	12 841	12 824	−17
$^4F_{7/2} + {}^4S_{3/2}$	13 446	13 448	2
	13 493	13 493	0
	13 588	13 592	4
	13 629	13 601	−29
	13 630		
	13 638	13 631	−7
	13 648	13 642	−6
$^4F_{9/2}$	14 738	14 750	12
	14 783	14 791	8
	14 805	14 804	−1
	14 856	14 870	14
	14 893	14 900	7
$^2H2_{11/2}$	15 983	15 969	−14
	15 995	15 987	−8
	16 003	16 014	11
	16 032	16 036	4
	16 044	16 046	2
	16 071	16 058	−13
$^4G_{5/2} + {}^2G1_{7/2}$	17 153	17 150	−3
	17 200	17 202	2
	17 299	17 297	−2
	17 347	17 348	1
	17 383	17 385	2
	17 425	17 427	2
	17 442	17 443	1
$^4G_{7/2}$	19 041	19 047	6
	19 081	19 087	6
	19 123	19 124	1
	19 225	19 216	−9
$^4G_{9/2} + {}^2K_{13/2}$	19 458	19 448	−10
	19 494	19 485	−9
	19 522	19 516	−6
	19 544	19 540	−4
	19 578	19 581	3
	19 590	19 594	4
	19 609	19 616	7
	19 649	19 645	−4
	19 688	—	—
	19 738	19 739	1
	19 826	19 829	3
	19 918	19 933	15
$^2G1_{9/2}$	21 043	21 062	19
	21 075	21 082	7
	21 107	21 097	−10
	21 143	21 141	−2
	21 168	21 159	−9
$^2D1_{3/2}$	21 228	21 228	0
	21 265	21 285	20
$^4G_{11/2} + {}^2K_{15/2}$	21 420	21 421	1
	21 458	21 465	7
	21 493	21 502	9
	21 528	21 525	2
	21 565	21 567	2
	21 598	—	—
	21 634	—	—
	21 660	—	—
	21 686	—	—
	21 712	—	—
	21 744	21 730	−14
	21 786	—	—
	21 822	21 821	−1
	21 904	21 898	−12
$^2P_{1/2}$	23 321	23 312	−9
$^2D1_{5/2}$	23 775	—	—
	23 890	—	—
	23 960	—	—
$^2P_{3/2}$	26 193	—	—
	26 293	—	—
$^4D_{3/2}$	28 036	28 039	3
	28 072	28 052	−20
$^4D_{5/2}$	28 203	28 204	1
	28 268	—	—
	28 410	28 416	6

[a] Nominal quantum numbers S, L, J for the atomic states associated with the group of multiplet states.

that due to the carboxylate and ether oxygen donor atoms in $Nd(oxydiacetate)^{3-}$ or O^{2-} ions in $NdAlO_3$.

5.2. Hamiltonian parameters

In view of a large number of complex CF parameters required for low symmetry systems, often an approximate higher symmetry is adopted to reduce the number of CFPs used for fittings. A common approach is to use e.g. C_2 instead of C_1 or C_i as well as C_{2v} instead of C_2 symmetry. In the system under consideration, an approximate C_2 axis is revealed

(figure 3(b)), if one rotates the axis system in a such way that the z-axis passes through the O(9) oxygen atom (from the water molecule, table 1). Note that for monoclinic symmetry one may choose the symmetry adopted axes (X, Y, Z) with respect to the monoclinic direction (C_2) in one of the three possible ways: $C_2 \parallel Z$, $C_2 \parallel Y$, or $C_2 \parallel X$ [7, 14]. Each case corresponds to a different CF Hamiltonian and thus yields a different set of CFPs. Thus, our choice corresponds to the case $C_2 \parallel Z$, which yields the non-zero CFPs with even $q = 0$, 2, 4, and 6. To check the validity of this approximation, the AOM calculated CFPs B_{kq} were transformed by appropriate rotations to the axis system with the approximate C_2 axis along the z-axis. If the monoclinic approximation was well obeyed, the non-monoclinic parameters Re B_{kq} and Im B_{kq} ($q = 1$, 3, 5) should approach zero. However, we find the values of these CFPs to be not negligibly small as compared to those with $q = 0$, 2, 4 and 6. Therefore, having no strong justification for a higher (monoclinic) symmetry approximation, we performed calculations based on the actual C_1 (triclinic) symmetry.

The AOM parameters e_μ^{O} determined in the initial step of our approach seem to be reliable and consistent with both the theoretical expectations and the data of others reported up to now [8–10]. The small errors indicate that they are well determined. Moreover, the three-parameter AOM approach describes the experimental energy levels very well. The largest difference between the measured and computed CF levels does not exceed 32 cm^{-1} and the rms deviation is as low as 13.2 cm^{-1} using the 85 experimental energies in fitting.

Note that the standardization procedure [11] applied here dealt with only the second-rank CFPs. Therefore, adjusting these CFPs first by a constraint fitting to experimental data is an indispensable step, which may alleviate, to a certain extent, the inherent shortcomings of AOM arising from the polarization of ligands and further neighbor contributions [8–10].

The 'optimized' CFPs B_{2q} are given in table 2 in the column denoted AOM–B_{kq}, together with B_{4q} and B_{6q} obtained directly from equation (9) using the modified AOM parameters, that is parameters with excluded contributions from second-rank CFPs. The two sets of {B_{20}, Re B_{21}, Im B_{21}, Re B_{22}, Im B_{22}} (in cm^{-1}), (1) {−86, −174, −236, −34, −270} obtained in the AOM step of the fitting and (2) {−112, −95, 276, 128, 212} after optimization, differ considerably, and so do the Euler angles required to reduce Re B_{21}, Im B_{21}, and Im B_{22} to zero for each CFP set. However, only a minor modification of the parameter s_2, from 256 to 247 cm^{-1}, is observed, which indicates that the two CFP sets have a similar modulus or 'norm' [7], whereas their orientation in the multiparameter space is different.

The existence of the correlated CFP datasets, i.e. the sets $S1$–$S6$ in table 2, may be turned into an advantage. Namely, these sets are utilized to improve the reliability of the final fitted results within the multiple correlated fitting technique (MCFT) originally proposed in [14] and extended in [7] and [15]. This is the cornerstone of the MCFT, which has been applied for the first time to several RE ion–host systems in [14]. The fittings performed using the sets $S1$–$S6$ (table 2) as the starting sets and varying all 24 CFPs turned out to converge into nearly the same solution (within the parameter uncertainty) after transformation into the standard range. Each fitted solution yields almost identical s_k value and the same rms deviation of 11.1 cm^{-1}. This indicates convincingly that the minimum closest to the starting point is well defined, with the starting point being near neither an inflection point nor a saddle point between multiple local minima.

The set averaged over six independently fitted sets, denoted Fit-avg in table 2, may be considered as the optimal final result of our CF analysis for the Nd^{3+} ion in $[Nd(hfa)_4(H_2O)](N(C_2H_5)_4)$. The optimization of the second-rank CFPs and the usage of the MCFT technique, based on several independent fittings in distinct CFP regions, support our assertion that this set corresponds to a global minimum and reduce the overall uncertainty of the final fitted CFP values [7].

One should be aware, however, that our calculations do not provide a direct proof that a global minimum was achieved in the fitting. Actually, fittings with other starting sets of B_{kq} parameters show that a multitude of minima with nearly the same goodness of fit may exist in the solution space. However, several attempts at fitting with random starting parameter sets (not reported here) yielded rms deviation larger than 11.1 cm^{-1}. Moreover, further calculations (also not reported here) in which starting values were determined using the superposition (SPM) model [34] yielded parameters almost identical, i.e. within the fitting errors, with our final Fit-avg CFP set.

It is worthwhile to notice also the agreement between our initial and final CFPs. Comparison of the values s_k obtained for the starting (AOM–B_{kq}) and fitted (Fit-avg) CFP sets reveals minor differences only: s_2, s_4 and s_6 are only slightly larger by 1.2, 2.6 and 0.7%, respectively, for the latter set as compared with the former set. For the CFP sets AOM–B_{kq} and Fit-avg the total crystal-field strength measured by the parameter s_{cf} also remains very similar, being equal to 328 and 333 cm^{-1}, respectively.

An inspection of the individual CFP values of the starting AOM–B_{kq} set, transformed to the standard $S4$ region, with the fitted set *Fit-avg* reveals that significant changes can be noticed only for Re B_{63} and Im B_{63}: the starting values are −248 and −242 cm^{-1}, whereas the fitted values are −537 and 245 cm^{-1}, respectively. Nevertheless, the closeness factors C_2, C_4, C_6 and the global factor C_{gl} [7] for the pair {S_4, Fit-avg} of the standardized CFP sets are 0.998, 0.922, 0.788 and 0.850, respectively. Thus the closeness factors as well as the similar values of the rotational invariants s_k and s_{cf} indicate remarkable consistence of the CFP sets obtained from the AOM step and those from the refined step. The maps of B_{40} and B_{60} parameters for $S4$ and Fit-avg sets presented in the next section clearly illustrate this observation.

Concluding, the CFP sets obtained independently in various fittings including six distinct Si regions of the multiparameter space as well as good overall compatibility of the refined CFPs and the AOM generated ones, makes our approach combining the initial AOM phase, optimization, and extended scanning of the parameter space very useful for analysis of optical spectra for rare-earth ions at low symmetry sites in crystals.

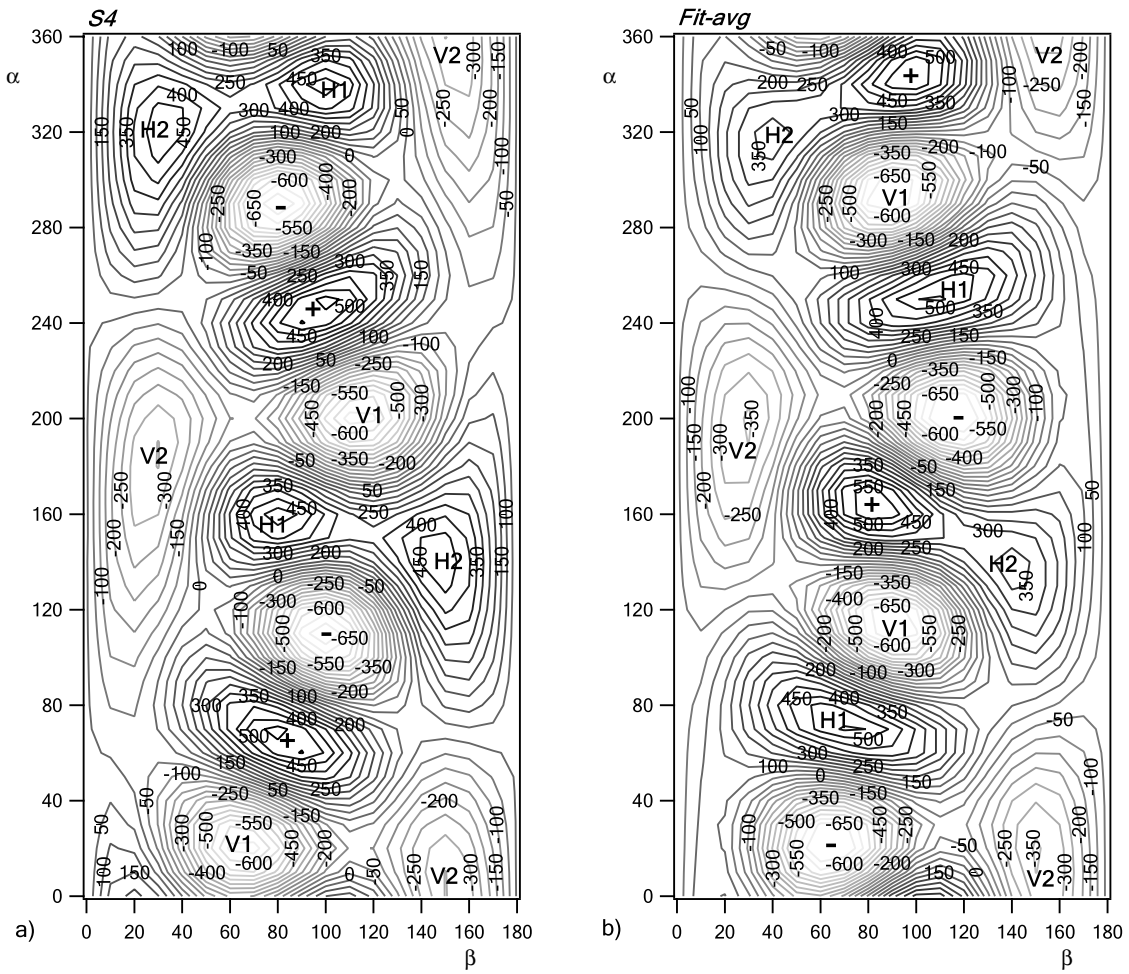

Figure 4. The maps of the B_{40} values (in cm^{-1}) for the CFP sets: (a) $S4$ and (b) Fit-avg of table 2, as functions of the reference frame rotation angles (see the text) α and β (in degrees). The signs '+' and '−' indicate the maximal and minimal points, respectively; the peaks are marked as $H1$ and $H2$, whereas the valleys as $V1$ and $V2$.

5.3. Nominal and crystallographic axis systems

In view of the existence of several physically equivalent solutions, each fitted CFP set must be considered as expressed in an undefined axis system, denoted in [7] as a '*nominal*' axis system. The actual orientation of the '*nominal*' axis system in a crystal for any fitted CFP set may be determined [7] by comparison of the fitted CFP set corresponding to a given region of the multiparameter space with the CFPs obtained from a theoretical model. In our AOM model calculations we adopt the crystallographic axis system—figure 3(a) and table 1. In general, the fitted CFP values may differ considerably from those used as the starting values, e.g. 'guessed' or theoretically computed as in our case. The most significant differences between our fitted (Fit-avg) and computed (AOM–B_{kq}) CFPs are observed for Re B_{63} and Im B_{63}. Due to the undetermined orientation of the '*nominal*' system for any fitted CFP set, it is not possible to assess how far any two CFP (fitted and computed) sets really differ from each other without calculation of the energy spectrum.

For this purpose the alternative representation of CFP sets may be very useful, namely, the maps of the axial CF parameters as a function of the Euler angles α and β running over all possible orientations of the '*nominal*' axis system. Originally the idea of mapping has been invoked in the context of the CFP standardization based on the maximum values of the axial CFPs [13].

Figures 4 and 5 present the maps of B_{40} and B_{60} for $[Nd(hfa)_4(H_2O)](N(C_2H_5)_4)$ as functions of axis system rotation angles α and β for the CFPs obtained in the initial AOM step and the refined CFPs, i.e. the $S4$ and Fit-avg sets of table 2. The highest peaks and the deepest valleys, corresponding to the maximal and minimal B_{k0} values, are indicated in the maps by '+' and '−', respectively. In the map of B_{40} for the $S4$ CFPs set, besides the point corresponding to the maximal B_{40} value, two other peaks may be identified in the range $0 \leqslant \alpha \leqslant \pi$, marked in figure 4(a) as $H1$ and $H2$ (ordered from 'higher' to 'lower'). Correspondingly, two additional valleys, labeled as $V1$ and $V2$ (with $V1$ being deeper than $V2$), are observed. Note that due to the translational symmetry of the maps the B_{k0} points at (α, β) and $(\alpha + \pi, \pi - \beta)$ angles are equivalent. Accordingly, the maps corresponding to the sets $S1$–$S6$ are exactly the same in the expanded Euler angle scheme. The mutual positions of the characteristic points '+', '−', $H1$, $H2$, etc may be considered as fingerprints distinguishing a given CFP set.

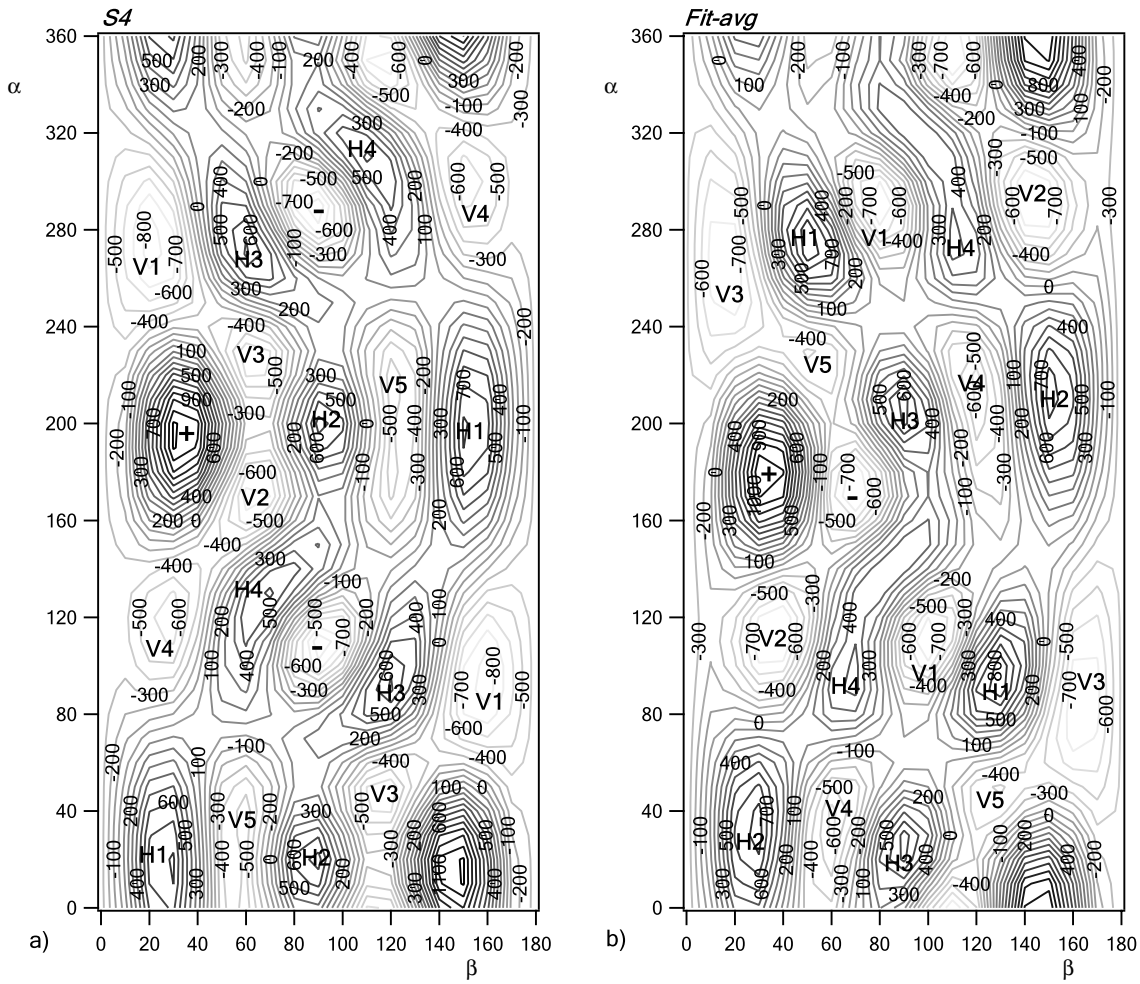

Figure 5. The maps of the B_{60} values (in cm^{-1}) for the CFP sets: (a) $S4$ and (b) Fit-avg of table 2, as functions of the reference frame rotation angles (see text) α and β (in degrees). The signs '+' and '−' indicate the maximal and minimal points, respectively; the peaks are marked as $H1$, $H2$, $H3$ and $H4$, whereas the valleys as $V1$, $V2$, $V3$, $V4$ and $V5$.

In general, the maps of B_{40} for the initial set $S4$ and the final (fitted) set Fit-avg, shown in figures 4(a) and (b), respectively, are very similar. The number of extreme points is the same and they occur at very closely positioned (α, β) points in each map. The maximal value in the B_{40} (Fit-avg) map occurs at a point very close to the second highest $H1$ peak in the $B_{40}(S4)$ map, whereas the $H1$ peak in the B_{40} (Fit-avg) map coincides with the maximal value of the $B_{40}(S4)$ map. Similarly, the minimal value of the B_{40} (Fit-avg) map matches very well that of the $V1B_{40}(S4)$ valley and the $V1$ valley in the B_{40} (Fit-avg) map corresponds very well to the minimal value of the $B_{40}(S4)$. The $H2$ peaks and $V2$ valleys occur in each map at very similar (α, β) coordinates.

Analogous similarities are also observed for the $B_{60}(S4)$ and B_{60} (Fit-avg) maps shown in figures 5(a) and (b), respectively. Hence, one may conclude that the occurrence of the peaks and valleys at similar positions in the $B_{k0}(S4)$ and B_{k0} (Fit-avg) maps reveals a very similar orientation of the distinguished z-axis of the 2^k-poles in H_{CF} obtained for the AOM calculated and then transformed CFPs ($S4$) and that for the fitted CFPs (Fit-avg). The observed changes in their relative magnitudes are due to adjustment of the calculated CFPs (set $S4$) to the experimental data in the fitting procedure. Therefore, one may expect that the '*nominal*' axis system (in which the fitted CFPs are obtained) differs from the crystallographic axis system (in which the atomic positions are expressed in table 1) due to the rotations required to set to zero the AOM−B_{kq}: Re B_{21}, Im B_{21}, and Im B_{22}, and the subsequent $S4$ transformation of the CFP set S_1 (see table 2). The combined transformation of the AOM–B_{kq} axis system into the $S4$ one is achieved by the following rotations (in degrees): ($\alpha = -36.72°$, $\beta = -77.37°$, $\gamma = -49.12°$), ($\alpha = 0$, $\beta = \pi/2$, $\gamma = 0$), and ($\alpha = \pi/2$, $\beta = 0$, $\gamma = 0$).

The similarities observed for $B_{k0}(S4)$ and B_{k0} (Fit-avg) maps illustrate the closeness between starting (AOM–B_{kq}) and fitted parameters, and thus additionally justify our choice of the final CFPs set (Fit-avg).

6. Summary and conclusions

The crystal-field (CF) analysis of optical absorption spectra measured at 4.2 and 298 K for Nd^{3+} ions in a $[Nd(hfa)_4(H_2O)](N(C_2H_5)_4)$ single crystal has been carried out for the actual C_1 symmetry of the metal ion site. The 85

energy levels of $4f^3$ configuration of Nd^{3+} have been assigned and determined from low temperature spectra. The energy level structure has been reproduced within rms deviation of 11.1 cm^{-1} using the seven free-ion parameters and 24 crystal-field ones of the conventional phenomenological Hamiltonian.

Only a few other CF calculations for Ln^{3+} ions at triclinic symmetry sites have been reported till now—for references see, e.g., [7, 11, 37]. To overcome the difficulties encountered in CF analysis for such low symmetry cases, we utilize the recent ideas concerning low symmetry CF parameterization [7, 11–13]. In brief, our procedure includes (i) the angular overlap model (AOM) [25, 10] calculations of the CF parameters (CFPs); (ii) an initial optimization fitting step of the AOM-determined second-rank CFPs; (iii) reduction of the number of independent CFPs [11, 14]; (iv) CFP standardization [7, 12, 14]; (v) application of the multiple correlated fitting technique (MCFT) [7, 14, 15] and additional scanning of the multidimensional parameter space; (vi) determination of the '*nominal*' axis systems associated with fitted CFP data sets [7]. We have also shown that the maps of the axial CF parameters B_{40} and B_{60} as functions of the Euler angles of rotation of the axis system may be useful for comparison of various low symmetry CFP sets, in particular, the initial CFP sets and the final ones fitted in the refining step. Each method adopted by us, i.e. the AOM calculations of the initial CFPs, the MCFT method, and the standardization idea, has already shown separately its merit and usefulness for crystal-field analysis [8–10, 15, 35, 36]. Here, these methods have been combined with the optimization of the second-rank parameters into one overall approach.

To make the problem of fitting tractable for a low symmetry system, the initial values of CF parameters need to be determined within simplified models with extremely reduce number of independent parameters, e.g. apart from AOM [25, 10] used in the present calculations, the exchange charge model (ECM) [37], the superposition model (SPM) [34], or the simple overlap model (SOM) [38]. The AOM has been shown previously [8–10] to have a sound basis in the quantum-chemical theory. Moreover, its accuracy can be determined relatively easily by estimation the induced electric multipole contributions to the CF potential [10, 39]. The CFPs calculated using the AOM model have to be transformed into the standardized form if they are to be used in the refined fitting using the general parametric Hamiltonian. Our analysis shows, however, that prior to this step it is advantageous to adjust additionally the second-rank CFPs B_{2q} by preliminary fitting to the experimental energy levels. This is consistent with the results of the *ab initio* calculations [8–10] that independently indicate the lowest accuracy of the CFPs determined within the AOM approximation for the second-rank CFPs.

An inadequate determination of the second-rank CFPs in the model calculations might result in inaccurately determined Euler angles, and consequently the fittings utilizing such ill determined initial CFPs might produce spurious minima. In this regard the MCFT technique [7, 14, 15] and additional scanning of the parameter space proved their usefulness in discrimination of the spurious minima in fittings of the CF energy levels to experimental data.

The idea of reduction of the number of independent CF parameters from the 27 CFPs admissible by group theory for triclinic symmetry to specific 24 CFPs, proposed in [11], has been used by us for analysis of absorption spectra for a low site-symmetry ion–host system. However, for meaningful fitting of 24 CFPs, a large number of experimental energy levels is still required. Fortunately, the simplified AOM approach provides an initial CFP set suitable for a satisfactory description of experimental energy levels yielding low rms deviation of 13.2 cm^{-1}. Such accuracy may be sufficient for prediction of energy levels not yet observed, which are required for calculations of energy transfer rates between ligands and lanthanide ion as well as evaluation of quantum efficiency of the given ion–host system. These aspects will be dealt with in a forthcoming paper.

In short, the CF model based on AOM determination of the starting values of the crystal-field parameters (CFPs) together with the refining steps lead to a reliable CFP set that allow us to reproduce the observed optical absorption spectra with high accuracy. Importantly, our approach may be utilized as a general framework for crystal-field analysis for other transition ions at low symmetry sites in crystals.

Acknowledgments

This work was partially supported by the research grants from the Polish Ministry of Science and Tertiary Education in the years 2006–2009 (projects No N204 066 31/1752 and 1 T09A 146 30) and the European Union—European Social Fund. One of the authors (A Mech) is the Polish Foundation for Science and the Max Born scholarships holder. The authors are grateful to Dr M Reid for providing us with the fitting program.

References

[1] Tang C and Vanslyka S A 1987 *Appl. Phys. Lett.* **51** 2902
[2] Burroughes J H, Bradley D D C and Holmes A B 1990 *Nature* **347** 539
[3] Lempicki A and Samelson H 1963 *Phys. Lett.* **4** 133
[4] de Sá G F, Malta O L, de Melo Donegá C, Simas A M, Longo R L, Santa-Cruz P A and da Silva E F Jr 2000 *Coord. Chem. Rev.* **196** 165
[5] Newman D J and Ng B 2000 *Crystal Field Handbook* (Cambridge: Cambridge University Press)
[6] Mulak J and Gajek Z 2000 *The Effective Crystal Field Potential* (Amsterdam: Elsevier)
[7] Rudowicz C and Qin J 2004 *J. Lumin.* **110** 39
[8] Gajek Z and Mulak J 1992 *J. Phys.: Condens. Matter* **4** 427
[9] Gajek Z 1995 *J. Alloys Compounds* **219** 238
[10] Gajek Z 2005 *Phys. Rev.* B **67** 045139
[11] Burdick G W and Reid M F 2004 *Mol. Phys.* **102** 1141
[12] Rudowicz C and Bramley R 1985 *J. Chem. Phys.* **83** 5192
[13] Mulak J and Mulak M 2005 *J. Phys. A: Math. Gen.* **38** 6081
[14] Rudowicz C 1986 *J. Chem. Phys.* **84** 5045
[15] Rudowicz C, Chua M and Reid M F 2000 *Physica* B **291** 327
[16] Wybourne B G 1965 *Spectroscopic Properties of Rare Earths* (New York: Interscience)
[17] Carnall W T, Crosswhite H, Crosswhite H M, Hessler J P, Edelstein N M, Conway J G, Shalimoff G V and Sarup R J 1980 *J. Chem. Phys.* **72** 5089
[18] Rudowicz C 1988 *Magn. Res. Rev.* **13** 1
Rudowicz C 1988 *Magn. Res. Rev.* **13** 335 (erratum)

[19] Rudowicz C 1985 *Chem. Phys.* **97** 43
[20] Yeung Y Y, Reid M F and Newman D J 2000 *Crystal Field Handbook* ed D J Newman and B Ng (Cambridge: Cambridge University Press) pp 254–258
[21] Linehan G J and Stedman G E 2001 *J. Phys. A: Math. Gen.* **34** 6663
[22] Gnutek P and Rudowicz C 2008 *Opt. Mater.* doi:10.1016/j.optmat.2008.05.013
[23] Rudowicz C and Gnutek P 2008 *J. Alloys Compounds* **456** 16
[24] Edmonds A R 1960 *Angular Momentum in Quantum Mechanics* (Princeton, NJ: Princeton University Press)
[25] Gerloch M 1983 *Magnetism and Ligand-Field Analysis* (Cambridge: Cambridge University Press)
[26] Chang N C, Gruber J B, Leavitt R P and Morrison C A 1982 *J. Chem. Phys.* **76** 3877
[27] Mech A 2008 *Polyhedron* **27** 393
[28] Rudowicz C 2000 *Crystal Field Handbook* ed D J Newman and B Ng (Cambridge: Cambridge University Press) pp 259–68
[29] Carnall W T, Goodman G L, Rajnak K and Rana R S 1989 *J. Chem. Phys.* **90** 3443
[30] Karbowiak M, Gajek Z and Drożdżyński J 2000 *J. Chem. Phys.* **261** 301
[31] Crosswhite H M, Crosswhite H, Kaseta F W and Sarup R 1976 *J. Chem. Phys.* **64** 1981
[32] May P S, Jayasankar C and Richardson F S 1989 *Chem. Phys.* **138** 123
[33] Quagliano J R, Burdick G W, Glover-Fischer D P and Richardson F S 1995 *Chem. Phys.* **321** 2001
[34] Newman D J and Ng B 1989 *Rep. Prog. Phys.* **52** 699
[35] Rudowicz C, Gnutek P and Karbowiak M 2007 *Phys. Rev.* B **76** 125116
[36] Loncke F, Zverev D, Vrielinck H, Khaidukov N M, Matthys P and Callens F 2007 *Phys. Rev.* B **75** 144427
[37] Malkin B Z 1987 *Spectroscopy of Solids Containing Rare-Earth* ed A A Kaplyanskii and B M Macfarlane (Amsterdam: North-Holland) p 33
[38] Malta O L 1982 *Chem. Phys. Lett.* **87** 27
Malta O L 1982 *Chem. Phys. Lett.* **88** 353
[39] Faucher M, Garcia D and Jorgensen C 1986 *Chem. Phys. Lett.* **129** 387